PCCP

PAPER

View Article Online
View Journal | View Issue

Cite this: *Phys. Chem. Chem. Phys.*, 2014, **16**, 22364

Vibrational spectra and structures of neutral Si_6X clusters (X = Be, B, C, N, O)†

Nguyen Xuan Truong,[a] Marco Savoca,[a] Dan J. Harding,[bc] André Fielicke[a] and Otto Dopfer*[a]

Received 31st July 2014,
Accepted 27th August 2014

DOI: 10.1039/c4cp03414g

www.rsc.org/pccp

Neutral silicon clusters doped with first row elements (Si_6X) have been generated (X = B, C, N, O) and characterized by infrared–ultraviolet (IR–UV) two-photon resonance-enhanced ionization spectroscopy (X = C, O) and quantum chemical calculations (X = Be, B, C, N, O, Si). In the near threshold UV photoionization, the ion signal of specific cluster sizes can be significantly enhanced by resonant excitation with tunable IR light prior to UV irradiation, allowing for the measurement of the IR spectra of Si_7, Si_6C, and Si_6O clusters. Structural assignments are achieved with the help of a global optimization procedure using density functional theory (DFT). The most stable calculated structures show the best agreement between predicted and measured spectra. The dopant atoms in the Si_6X clusters have a negative net charge and the Si atoms act as electron donors within the clusters. Moreover, the overall structures of the Si_6X clusters depend strongly on the nature of the dopant atom, *i.e.*, its size and valency. While in some of the Si_6X clusters one Si atom in Si_7 is simply substituted by the dopant atom (X = Be, B, C), other cases exhibit a completely different geometry (X = N, O). As a general trend, doping of the Si_7 cluster with first-row dopants is predicted to shift the optically allowed electronic transitions into the visible or even near-IR spectral range due to symmetry reduction or the radical character of the doped cluster.

I. Introduction

Small silicon clusters have attracted great interest in the current move towards nanoelectronics.[1] At the nanometer scale, where every atom counts, structure determination plays a crucial role. It has been shown that by changing the cluster size or dopant species, new stable nanostructures with tailored chemical, optical, or magnetic properties can be obtained.[2–8] While pure silicon clusters have been often studied as a test model system for quantum theories, doped silicon clusters have even more potential for applications in numerous fields of materials science.[9] Charged Si-containing clusters have been widely investigated, in part because they can be easily manipulated and detected using mass spectrometric methods. Gas-phase neutral clusters are more difficult to detect and thus less is known about them. Infrared photodissociation has been used for neutral clusters, in combination with ionization, to allow for mass spectrometric analysis of the cluster sizes.[10–12] Besides this, there have been two major spectroscopic methods used that directly influence the ionization process of the neutral clusters by absorption of IR photons, namely, infrared resonance-enhanced multiple photon ionization (IR–REMPI)[13] and infrared–ultraviolet two-color ionization (IR–UV2CI).[14] Generally, they are applied to cluster distributions and take advantage of the change in charge state resulting from photoionization of the cluster. In IR–REMPI, several hundred IR photons usually need to be absorbed in order to induce ionization. The method therefore works only for a limited range of very strongly bound systems like fullerenes and clusters of certain (refractory) metals and metal compounds.[13,15] The multiple photonic character can also make the interpretation of IR–REMPI spectra more difficult. Consequently, elaborate models have been applied to gain more insight into the multiple photon excitation mechanism.[16,17] IR–UV2CI, on the other hand, is more widely applicable. In IR–UV2CI experiments, a cluster first resonantly absorbs one or more IR photons to make a vibrational transition. It is then post-ionized by absorbing a single UV photon and finally detected in a mass spectrometer. The energy of the UV photon is chosen to be close to the ionization threshold, such that without the IR photons almost no ion signal is observed. Because only a few IR photons are involved in an IR–UV2CI measurement, the resulting vibrational spectra are closely related to the linear absorption spectra and hence much better resolved than typical IR–REMPI spectra. However, as the ionization energy (IE) of clusters is

[a] *Institut für Optik und Atomare Physik, Technische Universität Berlin, Hardenbergstraße 36, D-10623 Berlin, Germany. E-mail: dopfer@physik.tu-berlin.de*
[b] *Institut für Physikalische Chemie, Georg-August-Universität Göttingen, Tammannstraße 6, D-37077 Göttingen, Germany*
[c] *Department of Dynamics at Surfaces, Max-Planck-Institut für Biophysikalische Chemie, Am Faßberg 11, D-37077 Göttingen, Germany*

† Electronic supplementary information (ESI) available. See DOI: 10.1039/c4cp03414g

usually size-dependent, only selected cluster sizes may be probed with a given UV photon energy.

Whereas an enormous amount of theoretical work on small doped silicon clusters is available (*e.g.*, ref. 12, 18–34), only a few experiments have been reported in the gas phase.[8,14,35–38] By sequential doping of silicon clusters with carbon atoms, *i.e.*, for Si_mC_n with $m + n = 6$, we recently observed a systematic transition from one-dimensional geometries for pure C_6 to three-dimensional structures for pure Si_6.[38] In this study, we present complementary experimental and theoretical results on silicon clusters doped with first row elements (Si_6X, with X = Be, B, C, N, O). Structures of these clusters have been predicted using DFT-based basin hopping (BH) global optimization.[39,40] Refined DFT calculations have been performed for the most stable isomers, yielding detailed information such as vibrational spectra, excitation and ionization energies, HOMO–LUMO gaps, and natural charge populations. By comparing the IR–UV2CI spectra of Si_6C and Si_6O clusters to the calculations, the corresponding structures are assigned.

II. Experimental and computational methods

The experimental setup used for IR–UV2CI spectroscopy has been described in detail elsewhere.[14,38,41] Briefly, Si-rich Si_mX_n clusters are produced by laser ablation of a pure silicon rod within a pulsed flow of He gas (containing 1% CH_4, 0.7% N_2, or 0.07% O_2, depending on the desired dopant) and thermalized to ~100 K in a liquid-nitrogen cooled expansion channel. For the case of boron, a dual target source with pure He carrier gas is used.[42] After passing through a skimmer, the neutral Si_mX_n clusters are overlapped with counter-propagating IR radiation from the 'Free Electron Laser for Infrared eXperiments' FELIX and then post-ionized by an unfocused F_2 laser (7.87 eV) in the extraction zone of a reflectron time-of-flight mass spectrometer.

Fig. 1 shows typical mass spectra of the doped silicon clusters exposed to either UV only or the IR and UV lasers. The ion signal intensities depend strongly on the cluster size and the corresponding ionization energies. For clusters of specific sizes, with an IE close to the photon energy of the ionizing laser, prior resonant excitation with IR photons from a pulse of FELIX may enhance the ionization efficiency (Fig. 1d). Therefore, the enhancement of the ion yield as a function of the IR wavelength largely reflects the vibrational absorption spectrum of the original neutral cluster. Further details of the IR–UV ionization mechanism are provided in ref. 14 and 41.

The reported IR spectra are obtained from the relative ionization enhancement determined by the difference of the ion IR^{on} and IR^{off} signals normalized with the IR^{off} signal and the IR photon flux. The observed widths of the bands of 15–45 cm^{-1} arise from a combination of unresolved rotational structure, sequence hot band transitions involving low-frequency modes, the FELIX bandwidth (*ca.* 0.5–1% full width at half maximum (FWHM) of the central wavelength), and possibly the multiple photon absorption process.

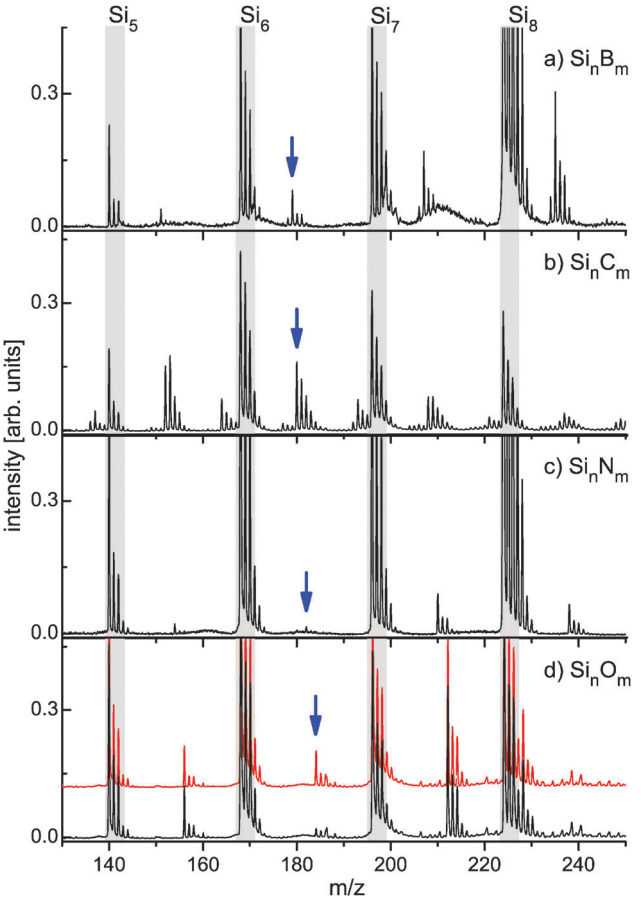

Fig. 1 Mass spectra (black lines) of doped silicon clusters Si_nX_m (n = 5–8, m = 1–2, and X = B, C, N, O) obtained by ionization with an F_2 laser. The Si_6X clusters are marked by arrows. For the case of oxygen (d), an additional mass spectrum (red line) is included to highlight the enhancement of the Si_6O ion yield with the presence of IR radiation at 865 cm^{-1}. For each group of signals, the leading mass peak corresponds to the all-^{28}Si isotopologue, while most of the adjacent peaks are assigned to other Si isotopologues.

Quantum chemical calculations have been performed to aid in the assignment of the cluster structures, to give more insight into their physical and chemical properties, and to serve as a guide for future experiments. By comparing the measured IR spectrum with the calculated spectra of the low lying isomers, the geometric structure of the observed cluster can be determined. Furthermore, an estimate of the IE of the clusters of interest is crucial for choosing the appropriate UV photon energy in the IR–UV2CI experiments.

For each cluster size, many geometric configurations are possible. In an effort to thoroughly explore these possibilities, we have employed the basin hopping technique,[40,43–46] which has proven to be an effective stochastic global search algorithm. Details of our implementation have been described elsewhere.[39] Basically, there are two main steps. First, for each cluster thousands of structures are evaluated in terms of the total energy by a BH algorithm coupled with DFT calculations at the RI-BP86/def-SVP level using Turbomole V6.3.1.[47–49] The BH uses a Monte Carlo (MC) simulation at a constant temperature

of 1200 K and consists of 1500 MC steps. New structures are generated with the significant structure variant using single-atom moves, followed by all-atom displacements at every five steps.[39] The self-consistent field (SCF) convergence criterium of 10^{-5} hartree on the total energy was chosen. The relatively low computational cost enables the BH approach to explore a large number of test structures. Second, the structures of interest, *e.g.*, the first 10–15 different low-energy isomers, are refined with different functionals, *i.e.*, the B3LYP/cc-pVTZ, TPSS/def2TZVP, and BP86/SVP levels, with SCF convergence conditions of better than 10^{-8} hartree and the resolution-of-the-identity approximation as implemented in the Gaussian 09 package.[50] We note that these methods have proven reliable for silicon-containing clusters reported previously.[14,38] At such levels, detailed information about the linear IR absorption spectra, ionization energies, and natural bond orbital populations is obtained. If not stated otherwise, all relative energies include zero-point vibrational energy corrections except for the vertical ionization energy (VIE) values. The electronic ground state of the considered clusters has the lowest possible spin multiplicity. The electronic transitions of the ground state structures are calculated at the CAM-B3LYP/cc-pVTZ level[50] to explore their electronic structure. To facilitate convenient comparison with the experimental spectra, the theoretical IR stick absorption spectra are convoluted with a Gaussian line profile using a FWHM of 15 cm^{-1}. The reported vibrational frequencies are unscaled.

III. Results and discussion

A. Predicted structures

The five lowest-energy isomers of the Si_6X clusters identified using the global optimization procedure described in Section II are shown in Fig. 2. The energetic, vibrational, and electronic parameters of the most stable isomers are listed in Tables 1–3, respectively. We note that the three functionals predict the same ground state structures while for higher-energy isomers the energetic ordering is only slightly changed. Therefore, the optimized geometric and vibrational parameters obtained with the B3LYP/cc-pVTZ level will be used in the following discussion.

Interestingly, for the most stable configurations of Si_6Be ($^1A_1$), Si_6B ($^2A'$), and Si_6C ($^1A_1$), the dopant atom simply replaces one Si atom of pure Si_7 (D_{5h}), leading to a reduction of the molecular symmetry. On the contrary, completely new structures are formed for Si_6N ($^2A_2$) and Si_6O (^1A). In most cases, the dopant atom prefers a location surrounded by as many Si atoms as possible. The Si_6O isomers are, however, most stable with an O atom on the edge of a low-energy isomer of the Si_6 cluster. Our numerical results are in good agreement with earlier calculations of Si_6O[24] and Si_6B.[51] Furthermore, to the best of our knowledge, we have found a new lowest-energy structure for the Si_6N cluster (**d0**, Fig. 2), which is significantly lower in energy (0.49 eV at the B3LYP/cc-pVTZ level) than the best structure reported previously (**d2**, Fig. 2 and, *e.g.*, ref. 52). While the **d2** structure is formed by the substitution of a Si atom, our new **d0** structure has a completely different geometry with only one Si atom attached to the divalent N atom, leading to an isocyanide-type linear configuration. Calculations with different methods, *e.g.*, genetic algorithms,[53] functionals, and basis sets (not shown here) support our finding.

If one only considers the substitutional isomers of Si_7, there are two possible places to exchange a Si atom for a dopant atom, namely, in the ring and at the apexes of the bipyramid. When located in the ring, Si_6Be, Si_6B, and Si_6N form C_{2v} symmetry isomers (**a0**, **b4**, and **d2**, Fig. 2), while Si_6C has C_s symmetry (**c3**, Fig. 2). When the dopant atom is placed at an apex of the bipyramid, Si_6C (**c0**, Fig. 2) and Si_6N (E_{rel} = 1.69 eV, not shown) form highly symmetrical configurations (C_{5v}), whereas the other clusters form lower symmetry C_s structures. The shortest Si–X bond lengths (in Å) in the most stable Si_6X structures are 2.16 (Be), 2.08 (B), 2.05 (C), 1.58 (N), and 1.66 (O).

B. Ionization energetics

The value of the ionization energy of a cluster compared to the UV photon energy used to finally ionize the cluster determines the success of an IR–UV2CI measurement. Experiments on neutral Si clusters suggest that the IE has to be within 0.1–0.2 eV of the UV photon energy to obtain sufficient enhancement in the ionization efficiency by resonant absorption of IR photons.[14,41] This also explains that in case of the Si_mC_n ($m + n = 6$) clusters no effect on the ionization efficiency of Si_3C_3 could be observed due to its high IE (9.12 eV) compared to the photon energy of 7.87 eV used for ionization.[38] The calculated adiabatic and vertical ionization energies and binding energies of the most stable Si_6X clusters with different functionals and basis sets are shown in Table 1. Note that our calculated values for Si_7 are in excellent agreement with experiments.[54,55]

Except for the case of Si_6N with a calculated VIE of $\sim$7.5 eV, the IEs of other clusters are close to the F_2 laser photon energy of 7.87 eV, making them promising candidates for IR–UV2CI spectroscopy using such a UV laser. Indeed, experimental IR–UV2CI spectra have been successfully recorded for Si_6C and Si_6O and are shown in Fig. 3. Si_6N may need a different experimental approach, as its predicted IE is too high for using an ArF laser (6.4 eV) and no other simple laser source exists in this UV range.

Finally, the binding energy (BE) of the dopant atom to the Si_6 cluster varies drastically between 2.2 and 8.7 eV depending on the nature of the dopant. While the BEs for the electropositive Be and B dopant atoms are similar or lower than that of Si, those of the more electronegative C, N, and O atoms are strikingly high ($\sim$8 eV).

C. Electronic properties

Mulliken populations are not very suitable for an analysis of the charge transfer in silicon clusters.[56] We have therefore used natural bond orbital concepts[57] to analyze the most stable Si_6X structures. The natural electronic configurations and natural populations are detailed in Table S1 in ESI.† For all of the dopants, the net atomic population is negative (−0.166 e (Be),

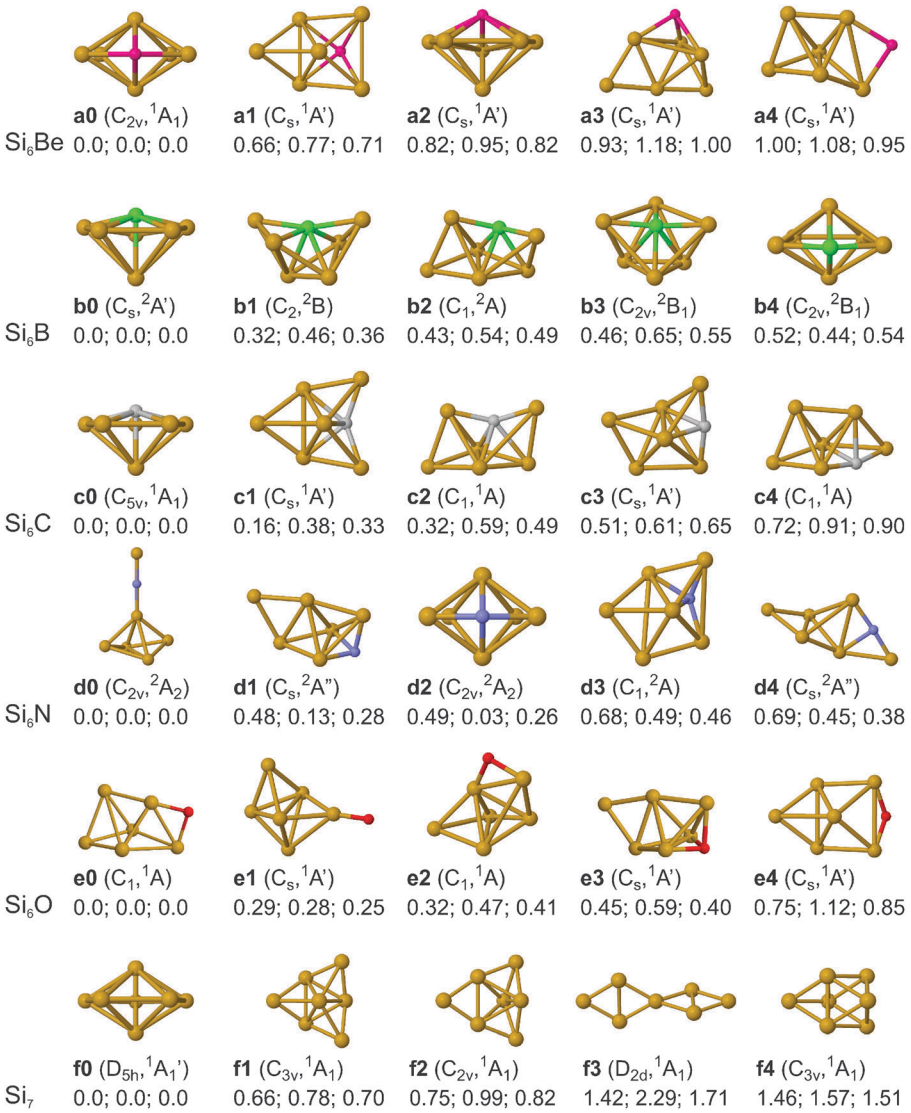

Fig. 2 Optimized geometries of the first five low-energy Si_6X isomers (with X = Be, B, C, N, O, Si) found with the global optimization algorithm. Point group symmetries and electronic states are given in parentheses. The relative energies E_{rel} (in eV) obtained at the B3LYP/cc-pVTZ, TPSS/def2TZVP, and BP86/SVP levels (separated by semicolons, left to right, respectively) are also provided for comparison. Atomic coordinates are available in the ESI.†

Table 1 Vertical ionization energy (VIE), adiabatic ionization energy (AIE), and binding energy (BE) of the lowest-energy Si_6X isomers (**a0**–**f0**) calculated at the B3LYP/cc-pVTZ, TPSS/def2TZVP, and BP86/SVP levels (separated by semicolons, left to right, respectively)

Cluster	VIE [eV]	AIE [eV]	BE[a] [eV]
Si_6Be	7.96; 7.54; 7.80	7.41; 7.37; 7.61	2.25; 2.59; 2.50
Si_6B	7.96; 8.22; 8.36	7.59; 7.75; 7.84	4.41; 4.76; 4.98
Si_6C	7.85; 7.82; 8.07	7.55; 7.66; 7.85	7.53; 7.94; 8.26
Si_6N	7.46; 7.57; 7.72	6.75; 6.93; 7.02	7.40; 5.31; 7.66
Si_6O	7.99; 8.02; 8.19	7.71; 7.74; 7.93	8.33; 8.69; 8.69
Si_7	7.98; 7.97; 8.23[b]	7.68; 7.71; 7.93[b]	4.84; 5.58; 5.40

[a] The binding energy of the Si_6X cluster is given as $BE = E(Si_6) + E(X) - E(Si_6X)$. [b] Experimental value is ~7.9 eV.[54,55]

−1.449 e (B), −1.884 e (C), −1.673 e (N), and −1.241 e (O)), hinting at the role as electron donors of Si atoms and the ionic characteristics of the Si–X bonding. This has also been observed for a number of silicon-containing clusters in earlier reports[56,58–60] and is attributed to the low electronegativity of Si. In terms of the natural electronic configurations, most of the dopants considered show an idealized promoted configuration for sp^3 hybridization, which is most preferable for Si atoms, except for the Be atom which has the valence configuration $2s^{0.66}2p^{1.45}$.

Excited states of the most stable Si_6X structures are calculated with the TD-DFT method (CAM-B3LYP/cc-pVTZ) as listed in Table 3 for the first three vertical electronic transitions along with the HOMO–LUMO gaps. The corresponding HOMO and LUMO orbitals are shown in Fig. 4. While the HOMO–LUMO gaps are comparable for all Si_6X, their first electronic transitions show a clear trend oscillating between closed- and open-shell clusters, *i.e.*, low excitation energies (0.5–1.2 eV) for open-shell *vs.* high values (>2.0 eV) for closed-shell systems. Interestingly,

Table 2 Vibrational frequencies (in cm^{-1}) of the most stable Si_6X isomers shown in Fig. 2 calculated at the B3LYP/cc-pVTZ level

Si_6Be (C_{2v})	Si_6B (C_s)	Si_6C (C_{5v})	Si_6N (C_{2v})	Si_6O (C_1)	Si_7 (D_{5h})
129 (0.6, a_1)	32 (0.6, a″)	105 (0, e_2)	71 (0.6, b_1)	75 (0.3, a)	159 (0, e_2″)
139 (0, a_2)	109 (0.1, a′)	231 (4, e_1)	74 (1.0, b_2)	120 (1, a)	216 (0.04, e_1′)
191 (0.3, b_1)	186 (1.0, a″)	261 (2, a_1)	157 (0.1, a_1)	192 (0.4, a)	217 (1, a_2″)
230 (6, b_2)	212 (9, a″)	274 (0, e_2)	204 (11, b_1)	234 (0.5, a)	271 (0, e_2′)
286 (0.2, b_2)	220 (3, a″)	355 (0.6, e_1)	234 (6, b_2)	240 (0.7, a)	320 (0, e_1″)
289 (2, b_1)	256 (0.1, a″)	421 (0, e_2)	236 (3, b_1)	272 (0.2, a)	333 (0, e_2′)
310 (2, a_1)	282 (0.5, a′)	432[A] (10, a_1)	264 (0, a_1)	285 (3, a)	350 (0, a_1′)
331 (3, a_1)	286 (2, a′)	552[B] (50, e_1)	291 (5, b_2)	316 (8, a)	404 (31, e_1′)
336 (0, a_2)	347 (0.1, a″)	553[B] (69, a_1)	304 (0.01, a_1)	363 (3, a)	421 (0, a_1′)
356 (1, a_1)	386 (0.1, a′)		319 (0, a_2)	376 (11, a)	
408 (3, b_1)	416 (13, a′)		403 (1, b_1)	403 (2, a)	
419 (13, b_2)	451 (0.2, a″)		415 (4, a_1)	422[D] (8, a)	
424 (15, a_1)	519 (33, a′)		471 (0.2, b_2)	466[E] (27, a)	
598 (8, a_1)	646 (29, a′)		665 (26, a_1)	572[F] (15, a)	
617 (0.04, b_2)	652 (28, a″)		1350 (330, a_1)	855[G] (80, a)	

IR intensities (in km mol^{-1}) and the symmetries of the modes are listed in parentheses. A–G: assigned bands determined by our experiments as shown in Fig. 3.

Table 3 The first three electronic transitions and HOMO–LUMO gaps for the ground state structures of Si_6X calculated with the CAM-B3LYP/cc-pVTZ method. The respective oscillator strengths f ($\times 10^{-3}$) are given in parentheses. For the open-shell Si_6B and Si_6N, the HOMO–LUMO gaps for α/β spin components are indicated by up/down arrows

Cluster	Transition energy [eV]	HOMO–LUMO gap [eV]
Si_6Be (**a0**, C_{2v}, $^1A_1$)	2.27 (0.0) 2.40 (5.7) 2.60 (0.4)	5.24
Si_6B (**b0**, C_s, $^2A'$)	0.52 (0.1) 1.10 (0.1) 1.25 (1.5)	6.45↑ 3.83↓
Si_6C (**c0**, C_{5v}, $^1A_1$)	2.62 (0.0) 3.37 (30.6) 3.48 (0.0)	5.64
Si_6N (**d0**, C_{2v}, $^2A_2$)	1.15 (0.0) 1.17 (0.7) 1.79 (9.7)	5.59↑ 4.33↓
Si_6O (**e0**, C_1, ^1A)	2.40 (0.9) 2.49 (3.6) 2.66 (11.8)	5.43
Si_7 (**f0**, D_{5h}, $^1A_1'$)	2.13 (0.0) 2.19 (0.0) 2.31 (0.0)	5.37

the HOMO–LUMO gaps drastically overestimate the energy of the lowest electronic transitions. High-symmetry structures exhibit several forbidden transitions. For instance, the first optically active state for Si_7 is the seventeenth excited state at 3.35 eV with an oscillator strength $f = 0.0082$.

At the first glance, the spatial distributions of the HOMO and LUMO are very different for each cluster. Furthermore, the HOMOs are localized at the Si atoms and not on the dopant. Clusters with similar topological geometries show similar HOMOs, *i.e.*, Si_6Be, Si_6B, Si_6C, and Si_7. For Si_6Be, Si_6C, and Si_7, the LUMOs are very similar, although the localization of the dopant atom within the cluster is different.

D. Vibrational spectra

Fig. 3 shows the calculated vibrational spectra of the most stable isomers of Si_6X (X = Si, C, O, Be, B, N), which are detailed in Table 2. Experimental spectra are available for Si_7, Si_6C, and Si_6O, allowing for a comparison with the spectra of the predicted isomers (Fig. 3a–c). In all three cases, the spectrum of the lowest-energy isomer shows the best agreement to the experimental one (see Fig. S1–S5 in ESI† for further IR spectra of higher-energy isomers). The result for Si_7 published earlier[14] is recalled here for completeness. The Si_7 spectrum shows a single band at 417 cm^{-1} that has been assigned to the intense doubly degenerate e_1' mode of the highly symmetric D_{5h} pentagonal bipyramidal structure.

Replacing one Si by a C atom in pure Si_7 significantly changes the IR–UV2CI spectrum (Fig. 3b). While the C-rich clusters prefer chain-like geometries, *e.g.*, SiC_6,[61] stable Si-rich clusters have 3D structures. The predicted **c0** structure of Si_6C has C_{5v} symmetry, which is deformed from the D_{5h} structure of Si_7 due to the greater strength of the C–Si bond *cf.* to Si–Si. The e_1' mode that dominates the spectrum of Si_7 has its counterpart in the e_1 mode for Si_6C. However, in Si_6C this mode is shifted to higher frequency, as it involves the lighter, but stronger bound C atom, and coincides with an intense a_1 mode that is not IR active in Si_7 (*cf.* Table 2). Together they can be assigned to the experimental band B. Similarly, the experimentally observed band A also corresponds to an a_1 mode that is not IR active in the pure Si_7 cluster. The band C at 664 cm^{-1} cannot be explained by the fundamental modes of the **c0** isomer, nor by any of the ten Si_6C isomers found within 1 eV in energy, suggesting that the band may be due to a combination band of the a_1 mode at 438 cm^{-1} with the low frequency modes at 231 cm^{-1} (e_1) or 261 cm^{-1} (a_1). The 3D structure of the most stable Si_6C isomer is in good agreement with our earlier findings for Si_mC_n ($m + n = 6$), where the first C atom does not change the topology of the geometry of the pure Si_6 cluster.[38]

The spectrum of Si_6O is dominated by an intense absorption band (G) centered at about 853 cm^{-1}. Comparison with the calculated spectrum of the **e0** isomer shows that the band is due to the symmetric stretch mode of the Si–O–Si bridge

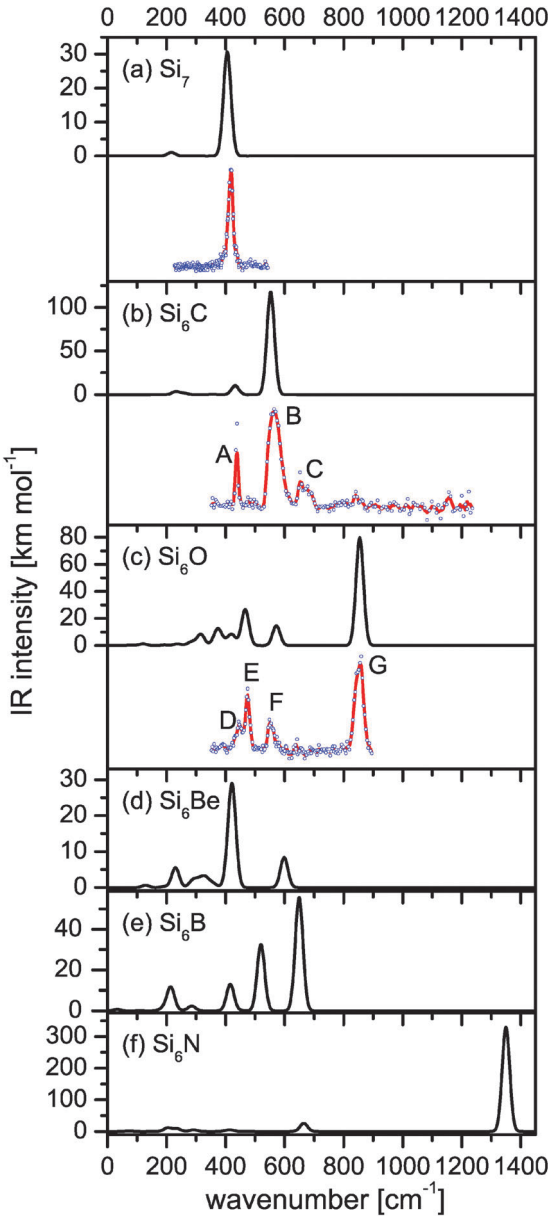

Fig. 3 IR spectra of the most stable isomers of Si_6X clusters (X = Si, C, O, Be, B, N) calculated at the B3LYP/cc-pVTZ level. The experimental IR spectra available for Si_7 (from ref. 14), Si_6C, and Si_6O are obtained by the IR–UV2CI technique (blue dots: original data; red lines: three-point adjacent average). The measured IR intensities are given on a linear scale in arbitrary units. The experimental line positions (in cm^{-1}) are 438 (A), 566 (B), 664 (C), 446 (D), 474 (E), 554 (F), and 853 (G).

predicted at 855 cm^{-1}. The asymmetric stretch vibration of the Si–O–Si unit is calculated at 572 cm^{-1} and can be assigned to the band F observed at 554 cm^{-1}.

For Si_6Be, Si_6B, and Si_6N, no experimental IR spectra have been obtained so far, but the calculated spectra are included for completeness. We refrain from a more detailed discussion here, but only point to the intense high-frequency band predicted for Si_6N (1350 cm^{-1}). This vibration is characteristic of the isolated silaisonitrile (–N═Si) group and can be compared to the Si–N stretch in H–N═Si found at ~1200 cm^{-1}.[62]

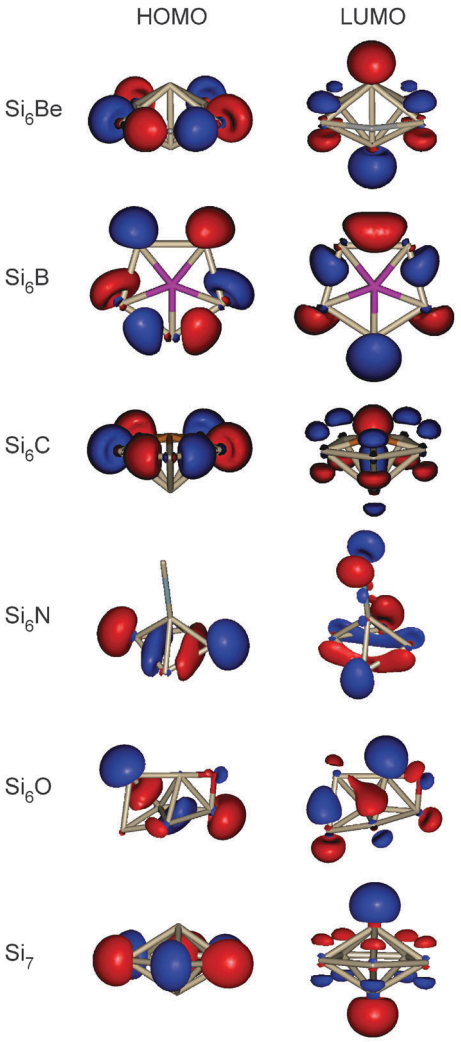

Fig. 4 HOMO and LUMO orbitals of the ground state structures of Si_6X shown in Fig. 2 (**a0**–**f0**). The structural orientations are adjusted for a clear illustration of the orbitals.

IV. Conclusions

In this study, neutral silicon clusters doped with the first row elements (B, C, N, O) have been generated in a laser vaporization source and characterized using time-of-flight mass spectrometry. The vibrational spectra of the C- and O-doped clusters have been measured using IR–UV2CI spectroscopy. The low energy structures of the Si_6X clusters doped with the first row elements Be–O have been investigated using DFT calculations. Candidate structures have been found using a DFT-based basin hopping global optimization scheme. In general, the most stable Si_6X structures and their IR spectra strongly depend on the dopant atom due to the effects arising from different size, mass, valency, and force fields. The calculations show that clusters doped with Be, B, or C favor structures based on the Si_7 pentagonal bipyramid, with substitution of a single Si atom in either the ring (Be) or at an apex (B, C). Si_6N and Si_6O, however, exhibit completely different structures. By comparison between the measured IR spectra and the predicted ones,

the structures of Si_6C and Si_6O have been determined. We find good agreement between the experimental and the calculated spectra of the lowest-energy isomers. The calculated ionization energies also appear to be reliable, providing useful information for future experiments on, *e.g.*, B and N doped clusters. Charge analysis with the natural bond orbital method shows that in all cases Si atoms act as electron donors within the clusters. As a general trend, doping of the Si_7 cluster with first-row dopants is predicted to shift the optically allowed electronic transitions into the visible range, which is partly ascribed to symmetry reduction or the radical character of the doped cluster. In particular, the open-shell Si_6B and Si_6N clusters have predicted absorptions in the near-IR spectral range. These theoretical predictions will guide our efforts in recording optical spectra of these doped silicon clusters. In addition, experiments with the dual-target laser ablation source are envisaged to record vibrational spectra of Si_nB.

Acknowledgements

This work was supported by the Deutsche Forschungsgemeinschaft within the research unit FOR 1282 (DO 729/5, FI 893/4). We gratefully acknowledge the support of the Stichting voor Fundamenteel Onderzoek der Materie (FOM) in providing beam time of FELIX and the FELIX staff for their skillful assistance, in particular, B. Redlich and A. F. G. van der Meer. The research leading to these results has received funding from the European Community's Seventh Framework Programme (FP7/2007–2013) under Grant Agreement No. 226716. We would like to acknowledge the collaboration with E. Janssens and P. Lievens using the dual target laser ablation cluster source. We thank C. Kerpal for fruitful discussion of the basin hopping technique.

References

1 V. Kumar, *Nanosilicon*, Elsevier Ltd, Oxford, 2007.
2 H. F. Li, X. Y. Kuang and H. Q. Wang, Probing the structural and electronic properties of lanthanide-metal-doped silicon clusters: M@Si_6 (M = Pr, Gd, Ho), *Phys. Lett. A*, 2011, **375**, 2836–2844.
3 S. Zhan, B. Li and J. Yang, Study of aluminum-doped silicon clusters, *Phys. B*, 2007, **387**, 421–429.
4 A. Titov, F. Michelini, L. Raymond, E. Kulatov and Y. A. Uspenskii, Gap narrowing in charged and doped silicon nanoclusters, *Phys. Rev. B: Condens. Matter Mater. Phys.*, 2010, **82**, 235419.
5 P. Karamanis, R. Marchal, P. Carbonniere and C. Pouchan, Doping-enhanced hyperpolarizabilities of silicon clusters: A global ab initio and density functional theory study of Si_{10}(Li, Na, K)$_n$ (n = 1, 2) clusters, *J. Chem. Phys.*, 2011, **135**, 044511.
6 L. Ma, J. Wang and G. Wang, Site-specific analysis of dipole polarizabilities of heterogeneous systems: Iron-doped Si_n (n = 1–14) clusters, *J. Chem. Phys.*, 2013, **138**, 094304.
7 V. T. Ngan, E. Janssens, P. Claes, J. T. Lyon, A. Fielicke, M. T. Nguyen and P. Lievens, High Magnetic Moments in Manganese-Doped Silicon Clusters, *Chem. – Eur. J.*, 2012, **18**, 15788–15793.
8 J. De Haeck, S. Bhattacharyya, H. T. Le, D. Debruyne, N. M. Tam, V. T. Ngan, E. Janssens, M. T. Nguyen and P. Lievens, Ionization energies and structures of lithium doped silicon clusters, *Phys. Chem. Chem. Phys.*, 2012, **14**, 8542–8550.
9 M. Jarrold, Nanosurface Chemistry on Size-Selected Silicon Clusters, *Science*, 1991, **252**, 1085–1092.
10 M. B. Knickelbein, The infrared photodissociation spectra of $Fe_n(CH_3OH)_m$ complexes and their deuterated analogs near 10μ, *J. Chem. Phys.*, 1996, **104**, 3517–3525.
11 P. Gruene, D. M. Rayner, B. Redlich, A. F. G. van der Meer, J. T. Lyon, G. Meijer and A. Fielicke, Structures of neutral Au_7, Au_{19}, and Au_{20} clusters in the gas phase, *Science*, 2008, **321**, 674–676.
12 M. Haertelt, J. T. Lyon, P. Claes, J. de Haeck, P. Lievens and A. Fielicke, Gas-phase structures of neutral silicon clusters, *J. Chem. Phys.*, 2012, **136**, 064301.
13 G. von Helden, D. van Heijnsbergen and G. Meijer, Resonant ionization using IR light: A new tool to study the spectroscopy and dynamics of gas-phase molecules and clusters, *J. Phys. Chem. A*, 2003, **107**, 1671–1688.
14 A. Fielicke, J. T. Lyon, M. Haertelt, G. Meijer, P. Claes, J. de Haeck and P. Lievens, Vibrational spectroscopy of neutral silicon clusters via far-IR-VUV two color ionization, *J. Chem. Phys.*, 2009, **131**, 171105.
15 V. J. F. Lapoutre, M. Haertelt, G. Meijer, A. Fielicke and J. M. Bakker, Communication: IR spectroscopy of neutral transition metal clusters through thermionic emission, *J. Chem. Phys.*, 2013, **139**, 121101.
16 A. Bekkerman, E. Kolodney, G. von Helden, B. Sartakov, D. van Heijnsbergen and G. Meijer, Infrared multiphoton ionization of superhot C_{60}: Experiment and model calculations, *J. Chem. Phys.*, 2006, **124**, 184312.
17 F. Calvo and P. Parneix, Amplification of anharmonicities in multiphoton vibrational action spectra, *ChemPhysChem*, 2012, **13**, 212–220.
18 G. Forte, G. G. N. Angilella, V. Pittala, N. H. March and R. Pucci, Neutral and cationic free-space oxygen-silicon clusters SiO_n ($1 < n \leq 6$), and possible relevance to crystals of SiO_2 under pressure, *Phys. Lett. A*, 2012, **376**, 476–479.
19 H. Ning, H. Fan and J. Yang, Probing the electronic structures and properties of neutral and charged $CaSi_n^-$ (n = 2–10) clusters using Gaussian-3 theory, *Comput. Theor. Chem.*, 2011, **976**, 141–147.
20 M. Jadraque and M. Martin, Charge-Transfer Processes in the Assembly of Si_nO_m Neutral Clusters, *J. Comput. Chem.*, 2011, **32**, 3497–3504.
21 Y. S. Wang and S. D. Chao, Structures and Energetics of Neutral and Ionic Silicon-Germanium Clusters: Density Functional Theory and Coupled Cluster Studies, *J. Phys. Chem. A*, 2011, **115**, 1472–1485.
22 H. Fan, Z. Ren, J. Yang, D. Hao and Q. Zhang, Study on structures and electronic properties of neutral and charged $MgSi_n^-$ (n = 2–10) clusters with a Gaussian-3 theory, *THEOCHEM*, 2010, **958**, 26–32.

23 Y. H. Zhu, B. X. Li, F. S. Liang and J. Xu, Theoretical Study of Neutral and Ionic Si_nO (n = 1–13) Clusters, *Int. J. Mod. Phys. B*, 2009, **23**, 3527–3536.
24 M. C. Caputo, O. Ona and M. B. Ferraro, Theoretical prediction of atomic and electronic structure of neutral Si_6O_m (m = 1–11) clusters, *J. Chem. Phys.*, 2009, **130**, 134115.
25 Y. Z. Lan and Y. L. Feng, Comparative study on the geometric and energetic properties, absorption spectra, and polarizabilities of charged and neutral $Cu@Si_n$ clusters (n = 9–14), *Phys. Rev. A: At., Mol., Opt. Phys.*, 2009, **79**, 033201.
26 D. Hossain, F. Hagelberg, C. U. Pittman, Jr. and S. Saebo, Structures and stabilities of clusters of Si_{12}, Si_{18}, and Si_{20} containing endohedral charged and neutral atomic species, *J. Phys. Chem. C*, 2007, **111**, 13864–13871.
27 R. Zhao, Z. Ren, P. Guo, J. Bai, C. Zhang and J. Han, Geometries and electronic properties of the neutral and charged rare earth Yb-doped Si_n (n = 1–6) clusters: A relativistic density functional investigation, *J. Phys. Chem. A*, 2006, **110**, 4071–4079.
28 C. Sporea, F. Rabilloud, A. R. Allouche and M. Frecon, Ab initio study of neutral and charged $Si_nNa_p^+$ ($n \leq 6$, $p \leq 2$) clusters, *J. Phys. Chem. A*, 2006, **110**, 1046–1051.
29 B. X. Li, Stability of medium-sized neutral and charged silicon clusters, *Phys. Rev. B: Condens. Matter Mater. Phys.*, 2005, **71**, 235311.
30 A. Sieck, T. Frauenheim and K. Jackson, Shape transition of medium-sized neutral silicon clusters, *Phys. Status Solidi B*, 2003, **240**, 537–548.
31 C. Xiao, F. Hagelberg and W. Lester, Geometric, energetic, and bonding properties of neutral and charged copper-doped silicon clusters, *Phys. Rev. B: Condens. Matter Mater. Phys.*, 2002, **66**, 075425.
32 S. Nayak, B. Rao, S. Khanna and P. Jena, Atomic and electronic structure of neutral and charged Si_nO_m clusters, *J. Chem. Phys.*, 1998, **109**, 1245–1250.
33 M. Gomei, R. Kishi, A. Nakajima, S. Iwata and K. Kaya, Ab initio MO studies of neutral and anionic SiC_n clusters (n = 2–5), *J. Chem. Phys.*, 1997, **107**, 10051–10061.
34 S. Wei, R. Barnett and U. Landman, Energetics and structures of neutral and charged Si_n ($n \leq 10$) and sodium-doped Si_nNa clusters, *Phys. Rev. B: Condens. Matter Mater. Phys.*, 1997, **55**, 7935–7944.
35 K. Koyasu, M. Akutsu, M. Mitsui and A. Nakajima, Selective formation of MSi_{16} (M = Sc, Ti, and V), *J. Am. Chem. Soc.*, 2005, **127**, 4998–4999.
36 K. Koyasu, J. Atobe, M. Akutsu, M. Mitsui and A. Nakajima, Electronic and geometric stabilities of clusters with transition metal encapsulated by silicon, *J. Phys. Chem. A*, 2007, **111**, 42–49.
37 P. Claes, V. T. Ngan, M. Haertelt, J. T. Lyon, A. Fielicke, M. T. Nguyen, P. Lievens and E. Janssens, The structures of neutral transition metal doped silicon clusters, Si_nX (n = 6–9; X = V, Mn), *J. Chem. Phys.*, 2013, **138**, 194301.
38 M. Savoca, A. Lagutschenkov, J. Langer, D. J. Harding, A. Fielicke and O. Dopfer, Vibrational Spectra and Structures of Neutral Si_mC_n Clusters ($m + n$ = 6): Sequential Doping of Silicon Clusters with Carbon Atoms, *J. Phys. Chem. A*, 2013, **117**, 1158–1163.
39 D. J. Harding, C. Kerpal, G. Meijer and A. Fielicke, Unusual Bonding in Platinum Carbido Clusters, *J. Phys. Chem. Lett.*, 2013, **4**, 892–896.
40 R. Gehrke and K. Reuter, Assessing the efficiency of first-principles basin-hopping sampling, *Phys. Rev. B: Condens. Matter Mater. Phys.*, 2009, **79**, 085412.
41 M. Haertelt, A. Fielicke, G. Meijer, K. Kwapien, M. Sierka and J. Sauer, Structure determination of neutral MgO clusters-hexagonal nanotubes and cages, *Phys. Chem. Chem. Phys.*, 2012, **14**, 2849–2856.
42 W. Bouwen, P. Thoen, F. Vanhoutte, S. Bouckaert, F. Despa, H. Weidele, R. Silverans and P. Lievens, Production of bimetallic clusters by a dual-target dual-laser vaporization source, *Rev. Sci. Instrum.*, 2000, **71**, 54–58.
43 D. Wales and J. Doye, Global optimization by basin-hopping and the lowest energy structures of Lennard-Jones clusters containing up to 110 atoms, *J. Phys. Chem. A*, 1997, **101**, 5111–5116.
44 M. Iwamatsu and Y. Okabe, Basin hopping with occasional jumping, *Chem. Phys. Lett.*, 2004, **399**, 396–400.
45 L. Zhan, J. Z. Y. Chen and W. K. Liu, Monte Carlo basin paving: An improved global optimization method, *Phys. Rev. E: Stat., Nonlinear, Soft Matter Phys.*, 2006, **73**, 015701.
46 M. T. Oakley, R. L. Johnston and D. J. Wales, Symmetrisation schemes for global optimisation of atomic clusters, *Phys. Chem. Chem. Phys.*, 2013, **15**, 3965–3976.
47 A. D. Becke, Density-functional exchange-energy approximation with correct asymptotic behavior, *Phys. Rev. A: At., Mol., Opt. Phys.*, 1988, **38**, 3098–3100.
48 J. P. Perdew, Density-functional approximation for the correlation energy of the inhomogeneous electron gas, *Phys. Rev. B: Condens. Matter Mater. Phys.*, 1986, **33**, 8822–8824.
49 F. Weigend, M. Haser, H. Patzelt and R. Ahlrichs, RI-MP2: optimized auxiliary basis sets and demonstration of efficiency, *Chem. Phys. Lett.*, 1998, **294**, 143–152.
50 M. J. Frisch, G. W. Trucks, H. B. Schlegel, G. E. Scuseria, M. A. Robb, J. R. Cheeseman, G. Scalmani, V. Barone, B. Mennucci, G. A. Petersson, H. Nakatsuji, M. Caricato, X. Li, H. P. Hratchian, A. F. Izmaylov, J. Bloino, G. Zheng, J. L. Sonnenberg, M. Hada, M. Ehara, K. Toyota, R. Fukuda, J. Hasegawa, M. Ishida, T. Nakajima, Y. Honda, O. Kitao, H. Nakai, T. Vreven, J. A. Montgomery, Jr., J. E. Peralta, F. Ogliaro, M. Bearpark, J. J. Heyd, E. Brothers, K. N. Kudin, V. N. Staroverov, R. Kobayashi, J. Normand, K. Raghavachari, A. Rendell, J. C. Burant, S. S. Iyengar, J. Tomasi, M. Cossi, N. Rega, J. M. Millam, M. Klene, J. E. Knox, J. B. Cross, V. Bakken, C. Adamo, J. Jaramillo, R. Gomperts, R. E. Stratmann, O. Yazyev, A. J. Austin, R. Cammi, C. Pomelli, J. W. Ochterski, R. L. Martin, K. Morokuma, V. G. Zakrzewski, G. A. Voth, P. Salvador, J. J. Dannenberg, S. Dapprich, A. D. Daniels, Ö. Farkas, J. B. Foresman, J. V. Ortiz, J. Cioslowski and D. J. Fox, *Gaussian 09 revision a.1*, Gaussian Inc., Wallingford, CT, 2009.
51 N. M. Tam, T. B. Tai and M. T. Nguyen, Thermochemical Parameters and Growth Mechanism of the Boron-Doped

Silicon Clusters, Si_nB^q with n = 1–10 and q = −1, 0, +1, *J. Phys. Chem. C*, 2012, **116**, 20086–20098.

52 J. Zh. Ye and B. X. Li, First-principles study on mixed Si_mN_n (m + n = 2–9) clusters, *Comput. Theor. Chem.*, 2012, **992**, 84–91.

53 D. E. Goldberg, *Genetic algorithms in search, optimization, and machine learning*, Addison-Wesley Professional, New York, 1989.

54 O. Kostko, S. R. Leone, M. A. Duncan and M. Ahmed, Determination of ionization energies of small silicon clusters with vacuum ultraviolet radiation, *J. Phys. Chem. A*, 2010, **114**, 3176–3181.

55 K. Fuke, K. Tsukamoto, F. Misaizu and M. Sanekata, Near threshold photoionization of silicon clusters in the 248–146 nm region: Ionization potentials for Si_n, *J. Chem. Phys.*, 1993, **99**, 7807–7812.

56 J. Han and F. Hagelberg, A density functional theory investigation of $CrSi_n$ (n = 1–6) clusters, *Chem. Phys.*, 2001, **263**, 255–262.

57 A. E. Reed, R. B. Weinstock and F. Weinhold, Natural population analysis, *J. Chem. Phys.*, 1985, **83**, 735–746.

58 C. Xiao and F. Hagelberg, Charge transfer mechanism in Cu-doped silicon clusters: a density functional study, *THEOCHEM*, 2000, **529**, 241–257.

59 J. Han and F. Hagelberg, A density functional investigation of $MoSi_n$ (n = 1–6) clusters, *THEOCHEM*, 2001, **549**, 165–180.

60 J. Han, C. Xiao and F. Hagelberg, Geometric and electronic structure of WSi_N (N = 1–6, 12) clusters, *Struct. Chem.*, 2002, **13**, 173–191.

61 V. Gordon, E. Nathan, A. Apponi, M. McCarthy, P. Thaddeus and P. Botschwina, Structures of the linear silicon carbides SiC_4 and SiC_6: Isotopic substitution and Ab Initio theory, *J. Chem. Phys.*, 2000, **113**, 5311–5320.

62 M. Chen, A. Zheng, H. Lu and M. Zhou, Reactions of atomic silicon and germanium with ammonia: A matrix-isolation FTIR and theoretical study, *J. Phys. Chem. A*, 2002, **106**, 3077–3083.

